Supporting Information for

Stereocontrolled Self-Assembly and Photochromic Transformation of Lanthanide Supramolecular Helicates

Li-Xuan Cai, Liang-Liang Yan, Shao-Chuan Li, Li-Peng Zhou and Qing-Fu Sun*†

†State Key Laboratory of Structural Chemistry, Fujian Institute of Research on the Structure of Matter, Chinese Academy of Sciences, Fuzhou 350002, People's Republic of China

Corresponding Email: qfsun@fjirsm.ac.cn

Contents

1. Synthetic Procedures

2. Supplemental Figures

Figure S1 ^{1}H NMR spectrum of **2** ($CDCl_3$, 400 MHz, 293 K). 3

Figure S2 ^{13}C NMR spectrum of **2** ($CDCl_3$, 100 MHz, 293 K). 4

Figure S3 ^{1}H NMR spectrum of ***o*-L^{RR}** (DMSO-d_6, 400 MHz, 293 K). 4

Figure S4 ^{1}H-^{1}H COSY NMR spectrum of ***o*-L^{RR}** (DMSO-d_6, 400MHz, 293K). 5

Figure S5 ^{13}C NMR spectrum of ***o*-L^{RR}** (DMSO-d_6, 100 MHz, 293 K). 5

Figure S6 ESI-TOF-MS spectrum for ligand ***o*-L^{RR}**. 6

Figure S7 ^{1}H NMR spectrum of **[Eu$_2$(*o*-L^{RR})$_3$](ClO$_4$)$_6$** (CD_3CN, 400 MHz, 293 K). 7

Figure S8 ^{1}H NMR spectrum of **[Eu$_2$(*o*-L^{SS})$_3$](ClO$_4$)$_6$** (CD_3CN, 400 MHz, 293 K). 7

Figure S9 ^{1}H-^{1}H COSY NMR spectrum of **[Eu$_2$(*o*-L^{RR})$_3$](ClO$_4$)$_6$** (CD_3CN, 400 MHz, 293 K). 8

Figure S10 ^{1}H NMR (400 MHz, CD_3CN, 298 K) titration spectra of titrating ***o*-L^{SS}** (3.3 mg/mL)with Eu(ClO_4)$_3$. 8

Figure S11 UV-Vis spectra of ***o*-L^{RR}** (3.0×10^{-5} M) when titrated with Eu(ClO_4)$_3$ in 2:3 v/v of $CHCl_3$/CH_3CN. 9

Figure S12 ^{1}H NMR (400 MHz, CD_3CN, 298 K) spectra of the complex Eu$_2$(***o*-L^{RR}**)$_3$(ClO_4)$_6$. The CD_3CN solution of the complex (a, [***o*-L^{RR}**] = 10 mg/mL) is diluted to the dilute solutions (b, [***o*-L^{RR}**] = 5 mg/mL and c, [***o*-L^{RR}**] = 1 mg/mL). 9

Figure S13 Simulated molecular models of four helicates based on *o*-L^{RR} ligands with the same metal centered chirality (*ΛΛ*). 10

Figure S14 ^{1}H NMR enantiomeric differentiation experiments for the enantiomers of (ΛΛ)-Eu$_2$(***o*-L^{RR}**)$_3$, and (ΔΔ)-Eu$_2$(***o*-L^{SS}**)$_3$ by addition of 3 equiv. chiral resolving agent Δ-TRISPHAT. 11

Figure S15 The photochromic process of the ligand **L^{RR}**. 11

Figure S16 ^{1}H NMR spectrum of *c*-**L^{RR}** ($CDCl_3$, 400 MHz, 293 K). 12

Figure S17 ^{1}H NMR spectrum of photochromic process of ligands ($CDCl_3$, 400 MHz, 293 K). 12

Figure S18 The photochromic process of the helicate [Eu$_2$(***o*-L^{RR}**)$_3$](ClO_4)$_6$. 13

Figure S19 ^{1}H NMR spectra of photochromic process of the helicate [Eu$_2$(***o*-L^{RR}**)$_3$](ClO_4)$_6$ (CD_3CN, 400 MHz, 293 K). 13

Figure S20 UV-Vis spectra changes of ***o*-L^{RR}** in $CHCl_3$ solution upon irradiation of 334 nm light (a) and corresponding ***c*-L^{RR}** upon irradiation of 630 nm light (b); UV-Vis spectra changes of Eu$_2$(***o*-L^{RR}**)$_3$(ClO_4)$_6$ in CH_3CN solution upon irradiation of 334 nm light (c) and corresponding Eu$_2$(***c*-L^{RR}**)$_3$(ClO_4)$_6$ upon irradiation of 630 nm light (d). 14

Figure S21 UV-Vis absorbance changes of Eu$_2$(***o*-L^{SS}**)$_3$(ClO_4)$_6$ in CH_3CN solution on alternate excitation at 334 and 630 nm over six cycles at 293 K. 14

Figure S22 CD spectra of the extracted ring-closed ligands ***c*-L^{RR}** (black line) and ***c*-L^{SS}** (red line) from the helicates (5×10^{-5} M, $CHCl_3$, 293K). 15

Figure S23 ESI-TOF-MS spectrum for the ring-closure helicate $Eu_2(\boldsymbol{c}\text{-}\mathbf{L}^{\boldsymbol{RR}})_3(ClO_4)_6$. 15

Figure S24 Excitation and emission spectra of $\boldsymbol{o}\text{-}\mathbf{L}^{\boldsymbol{SS}}$ (black) and corresponding ring-closure product $\boldsymbol{c}\text{-}\mathbf{L}^{\boldsymbol{SS}}$ upon irradiation of 334 nm in $CHCl_3$ (3×10^{-4} M)..... 16

Figure S25 Emission spectra of $Eu_2(\boldsymbol{o}\text{-}\mathbf{L}^{\boldsymbol{SS}})_3(ClO_4)_6$ and corresponding ring-closure product $Eu_2(\boldsymbol{c}\text{-}\mathbf{L}^{\boldsymbol{SS}})_3(ClO_4)_6$ in CH_3CN solution (1×10^{-4} M) (λ_{ex} = 270 nm)..... 16

Figure S 26 Emission spectra of ring-closure product $Eu_2(\boldsymbol{c}\text{-}\mathbf{L}^{\boldsymbol{SS}})_3(ClO_4)_6$ when exited at 441nm. 16

3. References

1. Synthetic Procedures

Synthesis of
4,4'-((4,4'-(perfluorocyclopent-1-ene-1,2-diyl)bis(5-methylthiophene-4,2-diyl))bis(ethyne-2,1-diyl))dianiline (2)

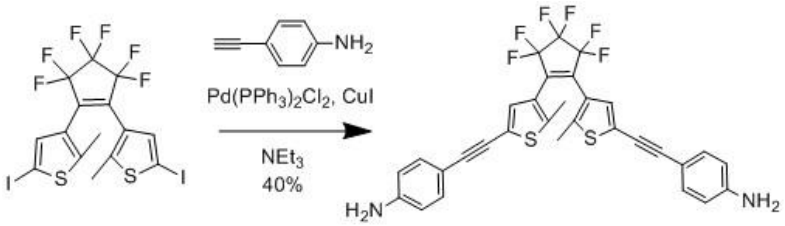

A mixture of perfluoro-1,2-bis(2-iodo-5-methylthien-4-yl)cyclopentene[S1] (620.1 mg, 1 mmol), 4-ethenylbenzenamine (351.4 mg, 3 mmol), CuI (28.6 mg, 0.15 mmol), $Pd(PPh_3)_2Cl_2$ (69.2 mg, 0.1 mmol) and degassed triethylamine (25 mL) was combined in an oven-dried Schlenk tube and stirred at 90 ℃ for 20 h. After removal of NEt3 by distillation, CH_2Cl_2 was added and the solution was washed with water and brine, dried over anhydrous $MgSO_4$ and concentrated in vacuo. The crude product was purified by column chromatography (silica) using CH_2Cl_2/ petroleum ether (1:1) as eluents to give a green solid (239.4 mg, 0.4 mmol) in 40% yield. ^{1}H NMR (400 MHz, $CDCl_3$) δ 7.31 (d, J = 8.6 Hz, 4H), 7.18 (s, 2H), 6.63 (d, J = 8.6 Hz, 4H), 3.86 (s, 4H), 1.91 (s, 6H). ^{13}C NMR (101 MHz, $CDCl_3$) δ 147.08 (s), 142.63 (s), 133.17 (s), 130.57 (s), 124.74 (s), 122.69 (s), 114.82 (s), 111.81 (s), 94.82 (s), 79.45 (s), 14.61 (s). HR-MS (ESI) calcd for $C_{31}H_{20}F_6N_2S_2$ $[M+H]^{1+}$: 599.1045, found 599.1040.

2. Supplemental Figures

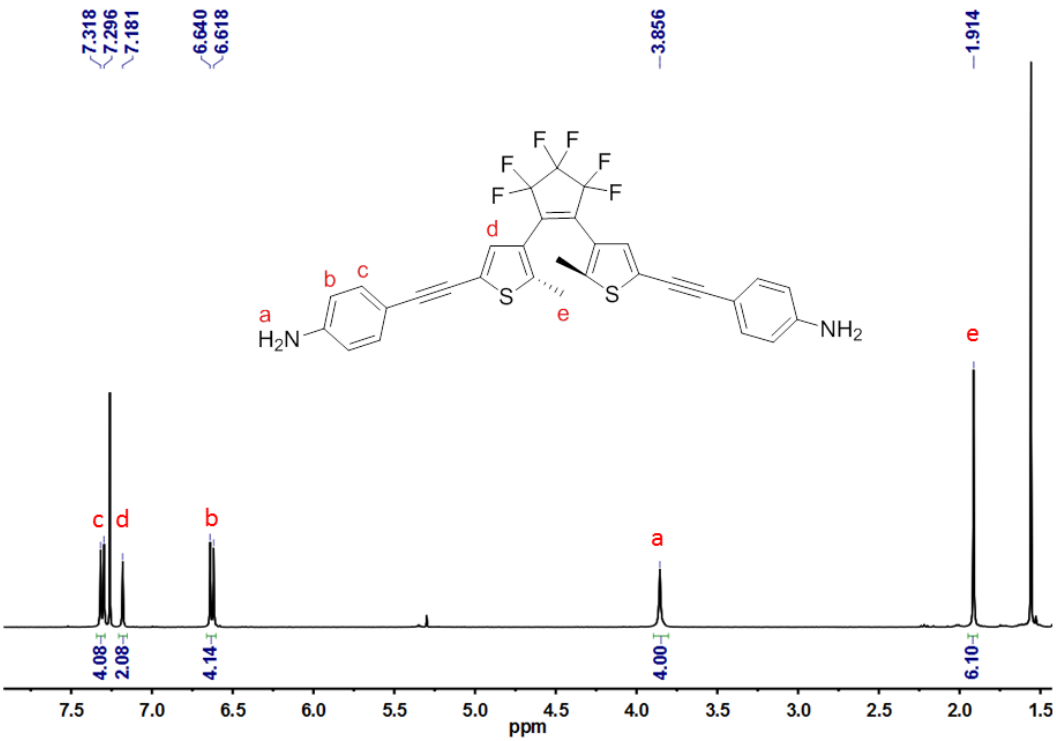

Figure S 1 ^{1}H NMR spectrum of **2** ($CDCl_3$, 400 MHz, 293 K).

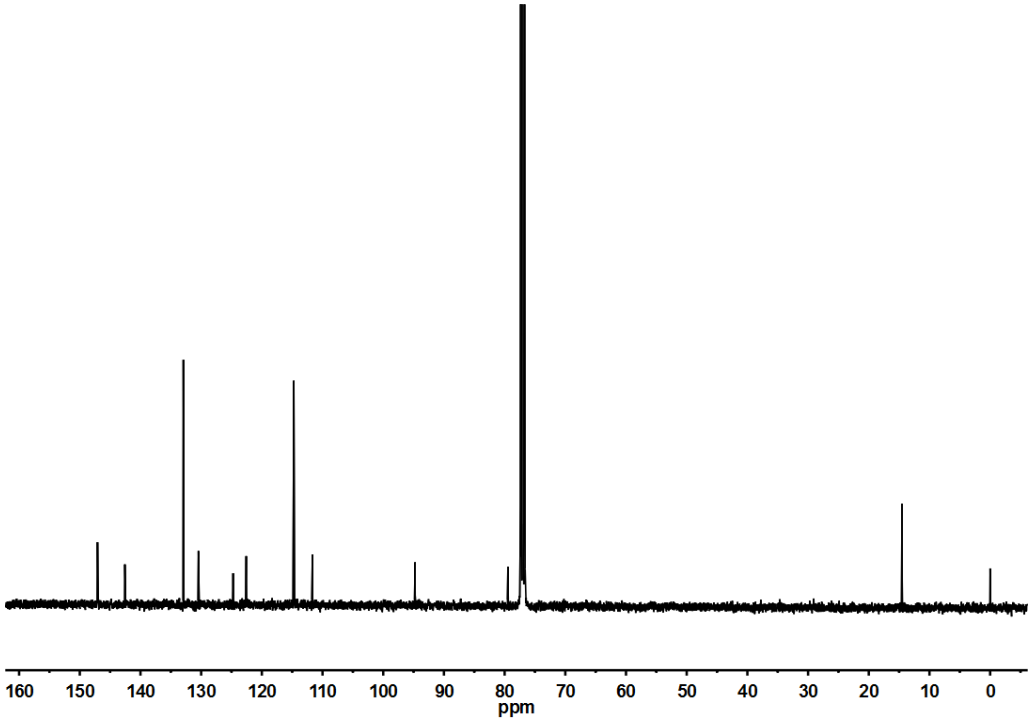

Figure S 2 ^{13}C NMR spectrum of **2** ($CDCl_3$, 100 MHz, 293 K).

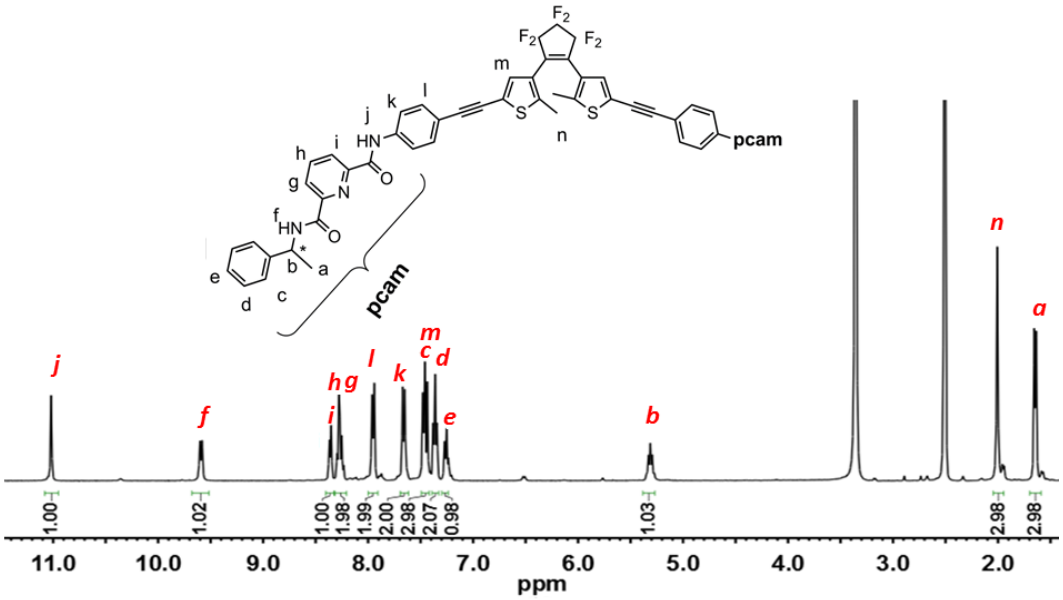

Figure S 3 ^{1}H NMR spectrum of ***o*-L^{RR}** (DMSO-d_6, 400 MHz, 293 K).

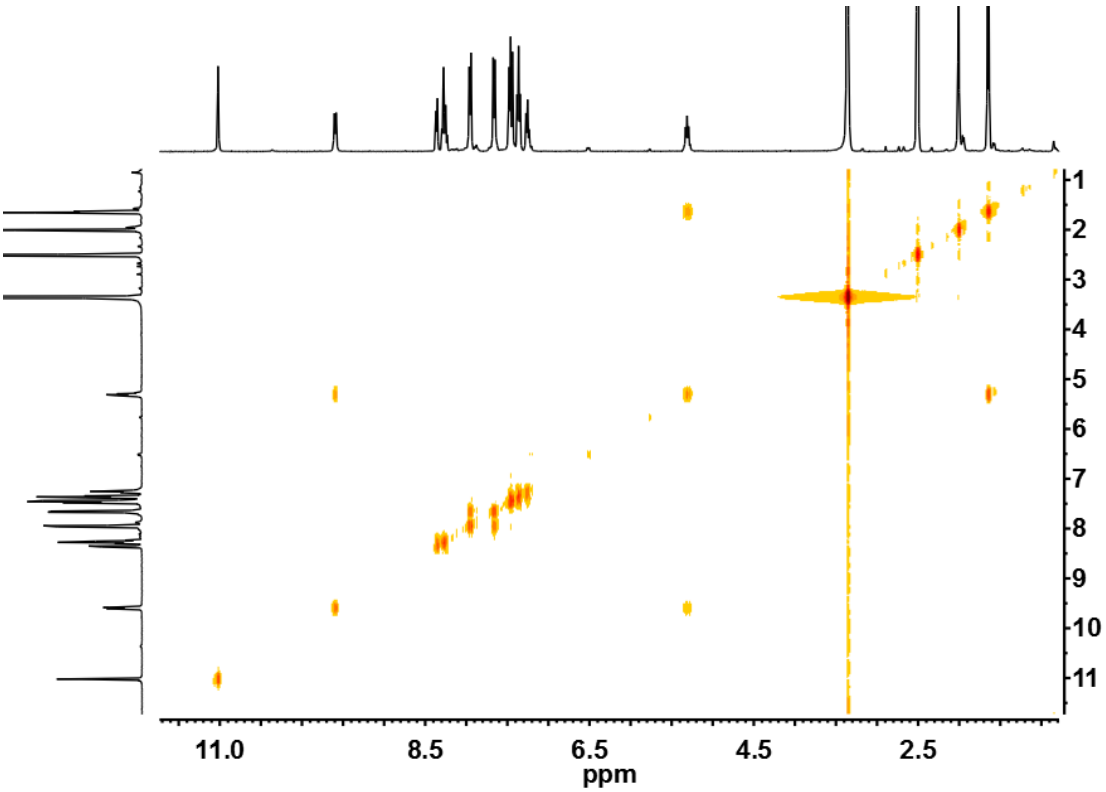

Figure S 4 ^{1}H-^{1}H COSY NMR spectrum of ***o*-L^{RR}** (DMSO-d_6, 400MHz, 293K).

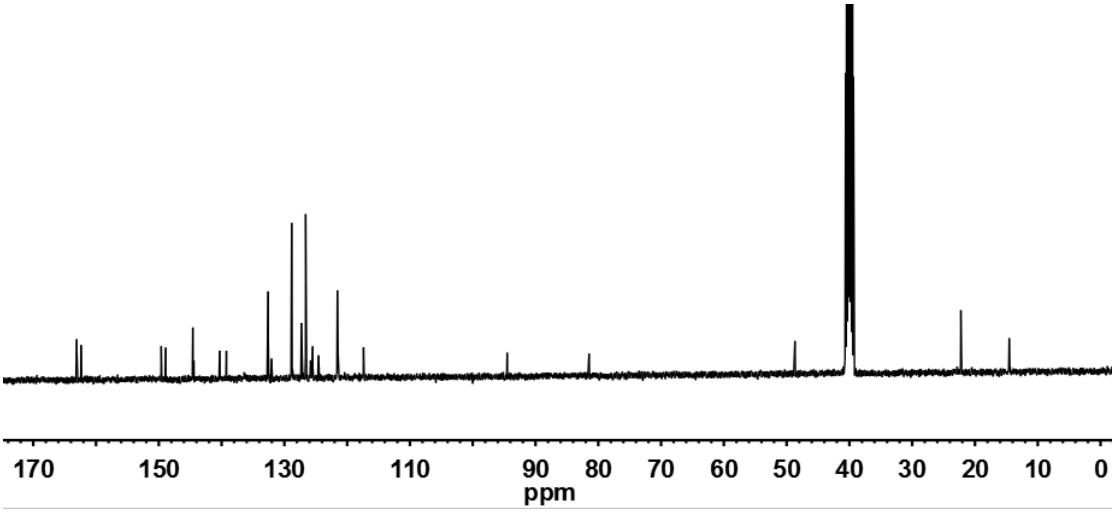

Figure S 5 ^{13}C NMR spectrum of ***o*-L^{RR}** (DMSO-d_6, 100 MHz, 293 K).

Generic Display Report

Analysis Info

Analysis Name	F:\YanLL_paper-4-dTe\MASS\CLX-LRR_2-A,3_01_18352.d	Acquisition D	2018-5-3 22:32:18
Method	pos-sqf-ligand-ms-pos-200-2000-1.m	Operator	BDAL@DE
Sample Name	CLX-LRR	Instrument	impact II
Comment			

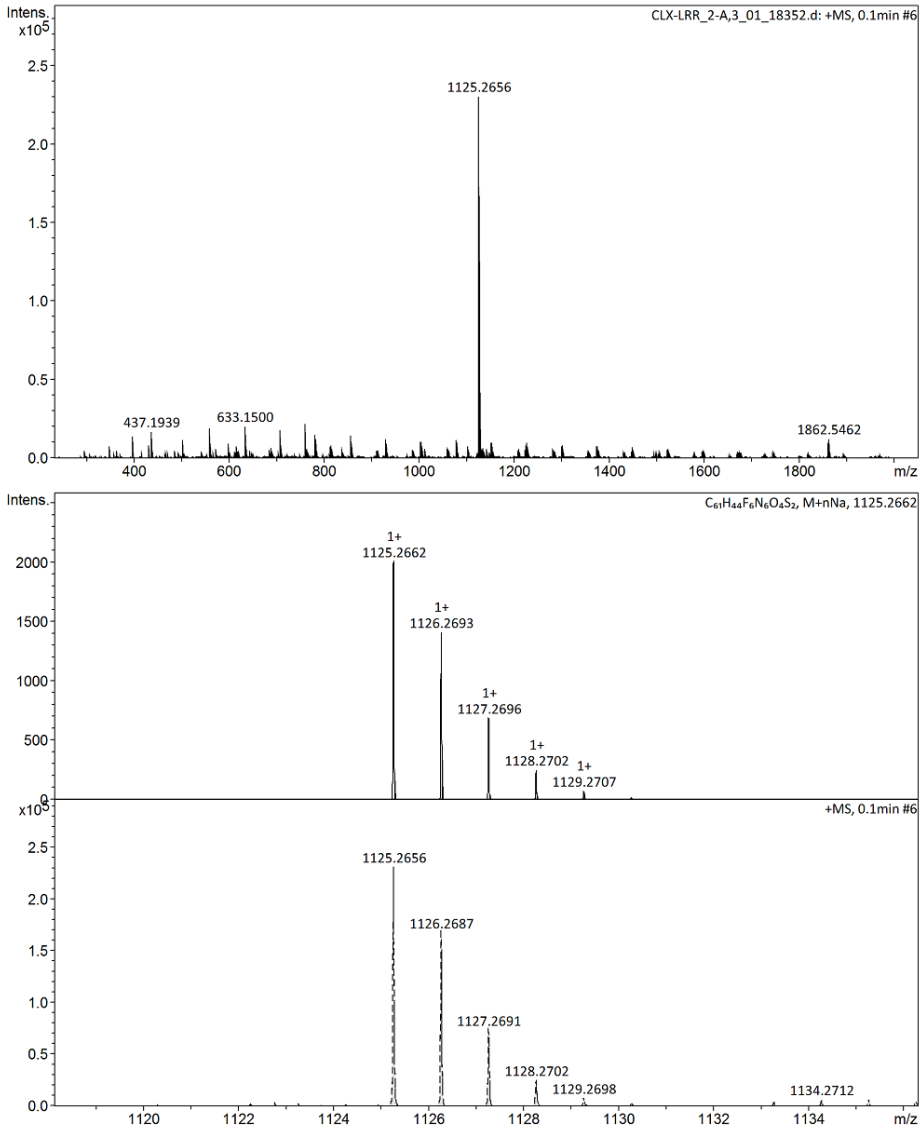

Bruker Compass DataAnalysis

Figure S 6 ESI-TOF-MS spectrum for ligand ***o*-L^{RR}**.

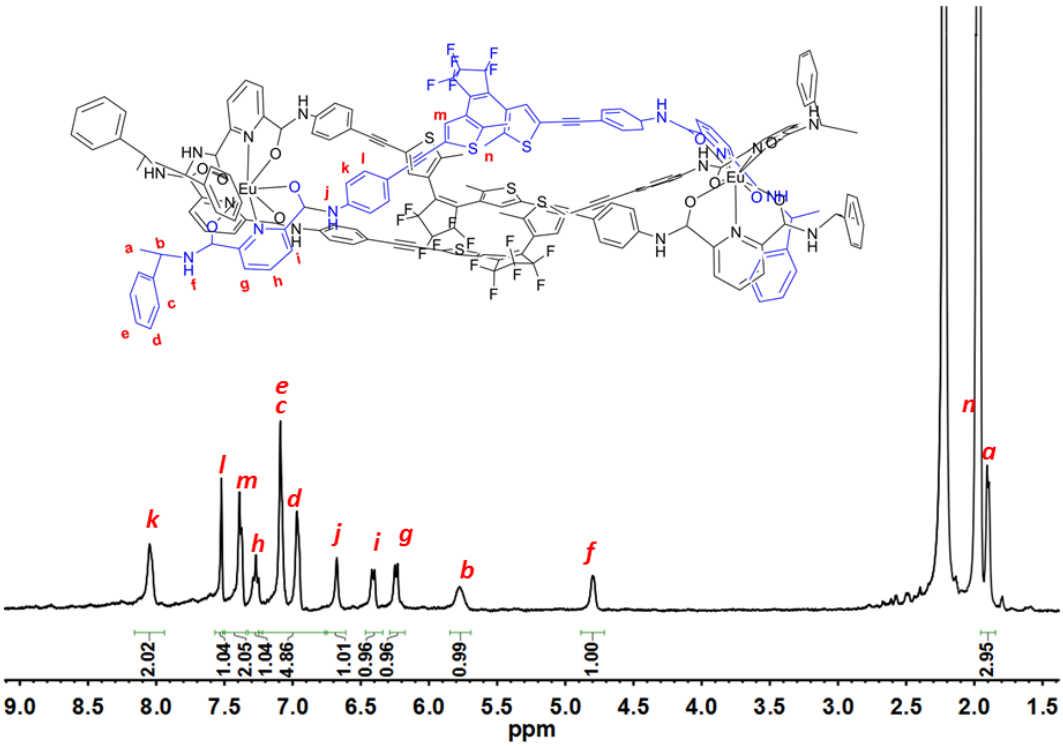

Figure S 7 ^{1}H NMR spectrum of **[Eu$_2$(*o*-L^{RR})$_3$](ClO$_4$)$_6$** (CD_3CN, 400 MHz, 293 K).

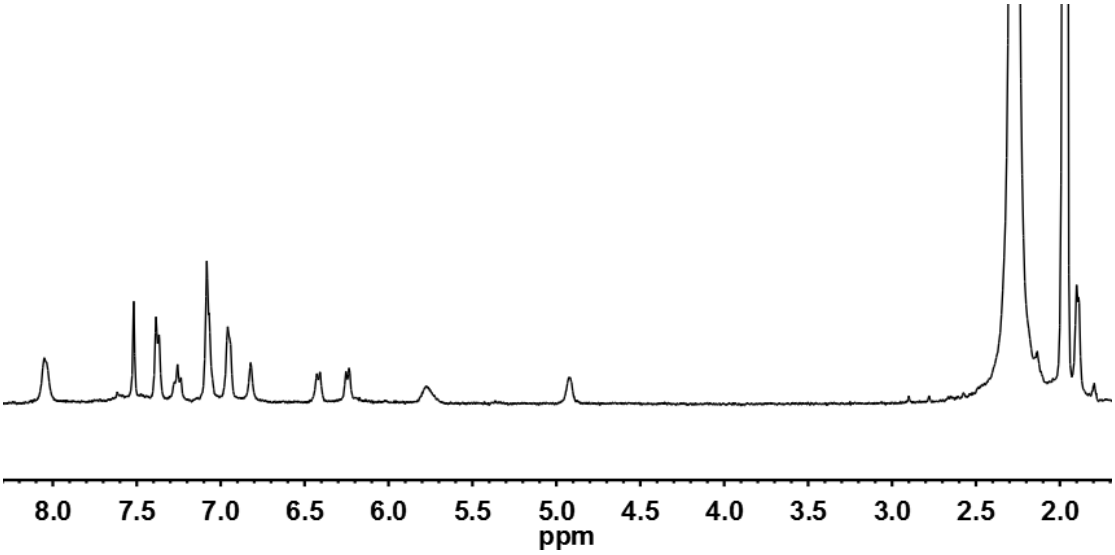

Figure S 8 ^{1}H NMR spectrum of **[Eu$_2$(*o*-L^{SS})$_3$](ClO$_4$)$_6$** (CD_3CN, 400 MHz, 293 K).

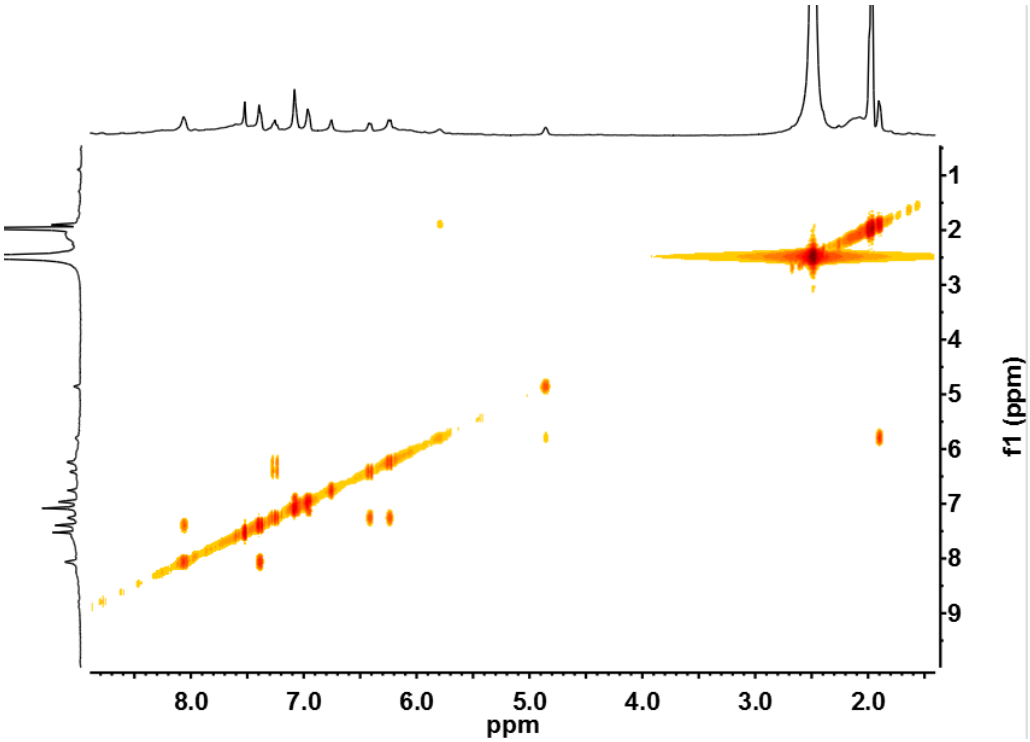

Figure S 9 ^{1}H-^{1}H COSY NMR spectrum of **[Eu$_2$(*o*-L^{RR})$_3$](ClO$_4$)$_6$** (CD$_3$CN, 400 MHz, 293 K).

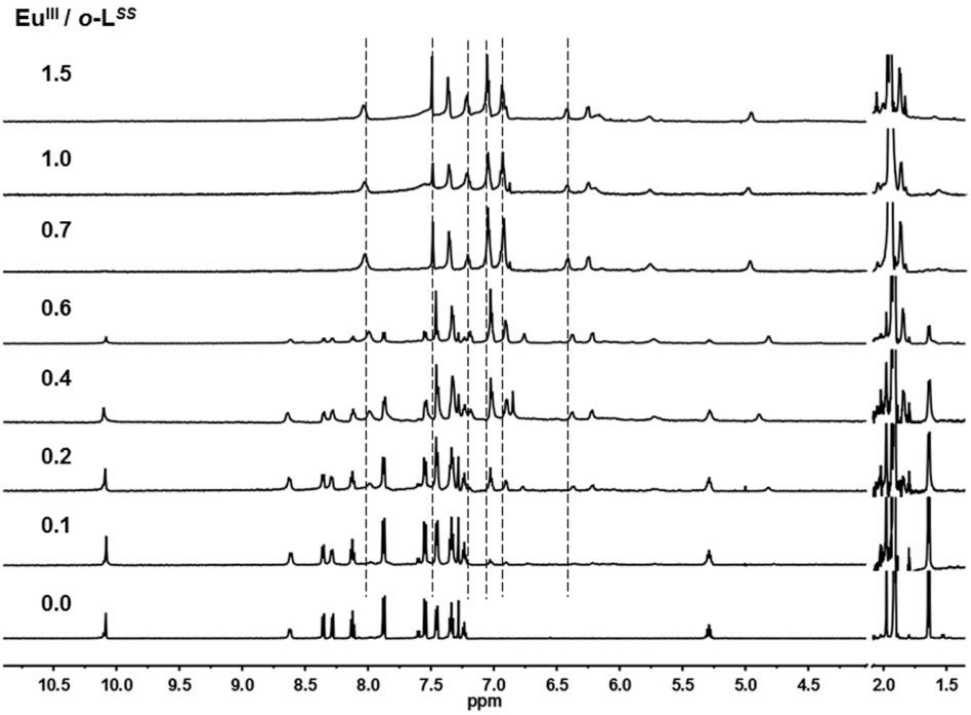

Figure S 10 ^{1}H NMR (400 MHz, CD$_3$CN, 298 K) titration spectra of titrating ***o*-L^{SS}** (3.3 mg/mL)with Eu(ClO$_4$)$_3$ with M/L ratio varying from 0 to 1.5.

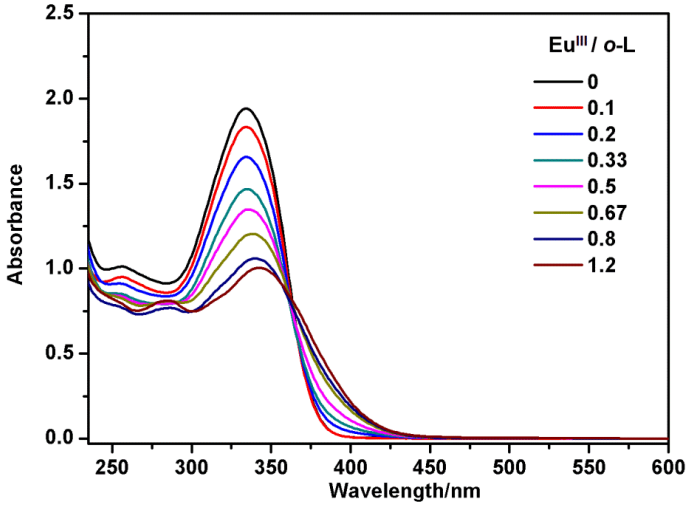

Figure S 11 UV-Vis titration spectra for ligand ***o*-L^{RR}** (3.0 × 10^{-5} M; 2:3 v/v of $CHCl_3/CH_3CN$) and $Eu(ClO_4)_3$ with M/L ratio varying from 0 to 1.2.

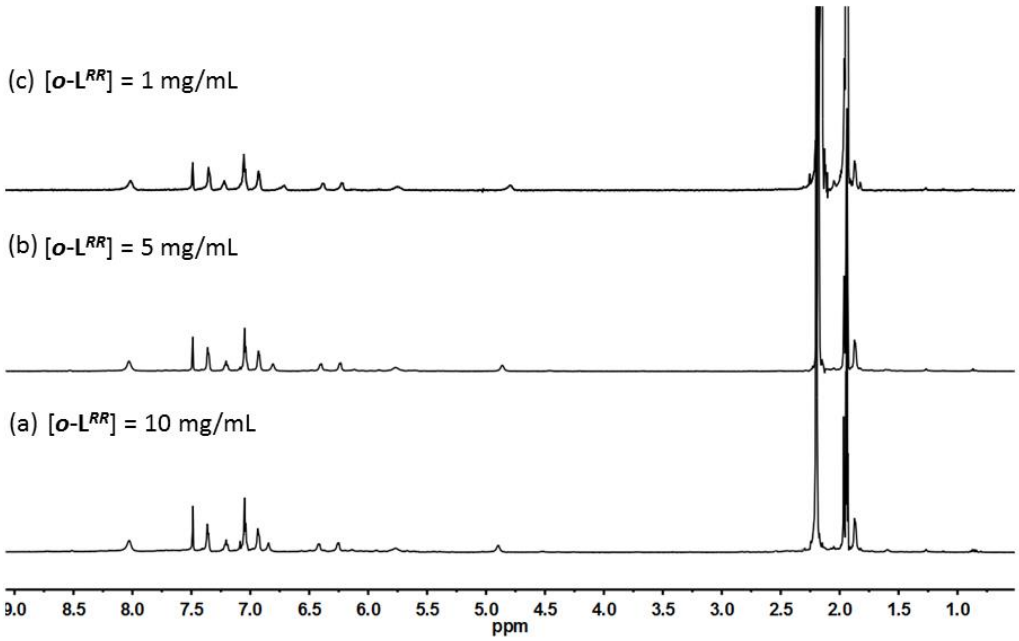

Figure S 12 ^{1}H NMR (400 MHz, CD_3CN, 298 K) dilution spectra of the complex Eu_2(***o*-L^{RR}**)$_3(ClO_4)_6$ at different ligand concentration [***o*-L^{RR}**] = 10 mg/mL (a), 5 mg/mL (b) and 1 mg/mL (c).

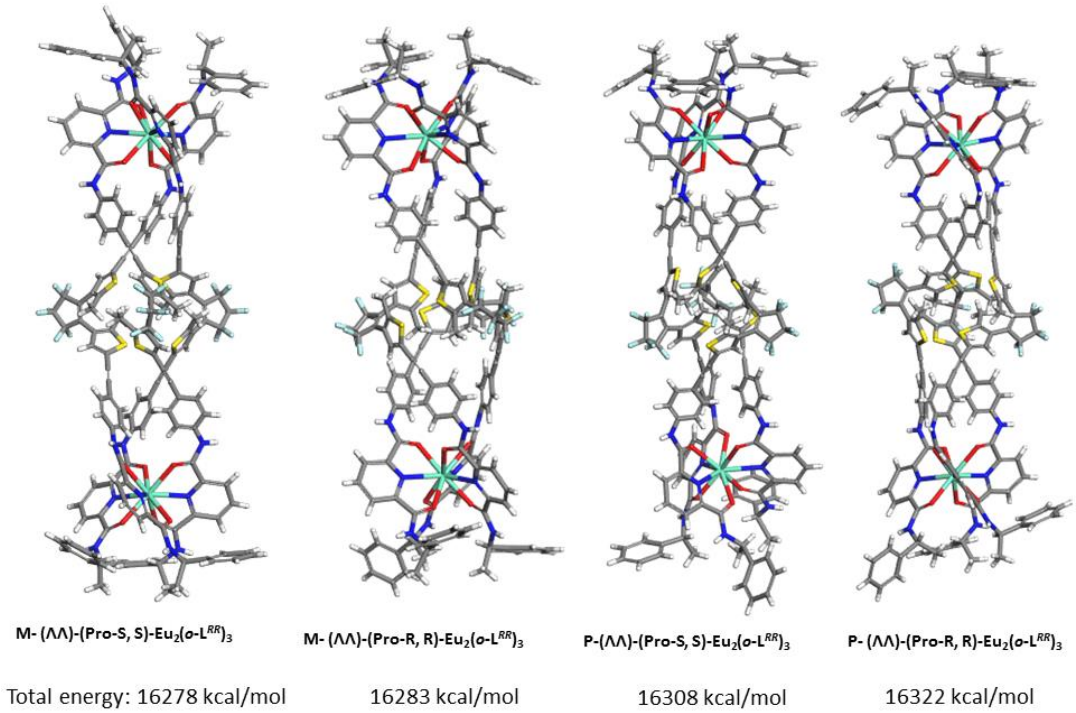

Figure S 13 Simulated molecular models of four helicates based on *o*-L^{RR} ligands with the same metal centered chirality (*ΛΛ*). The molecular mechanic modeling by Materials Studio program was employed to optimize the structures. First, we imported the crystal structure with the same chiral-inducing group and metal stereogenic center into the program and then changed the center linkers to our DTE units. We kept the periphery metal stereogenic center as rigid Motion Groups and only central DTE units are geometrically optimized. Based on the energy differences between the final optimized structure for the four possible conformational isomers as shown above, the M-(ΛΛ)-(pro-*S*, *S*)-Eu_2(***o*-L^{RR}**)$_3$ isomer was obtained as the most reasonable structure.

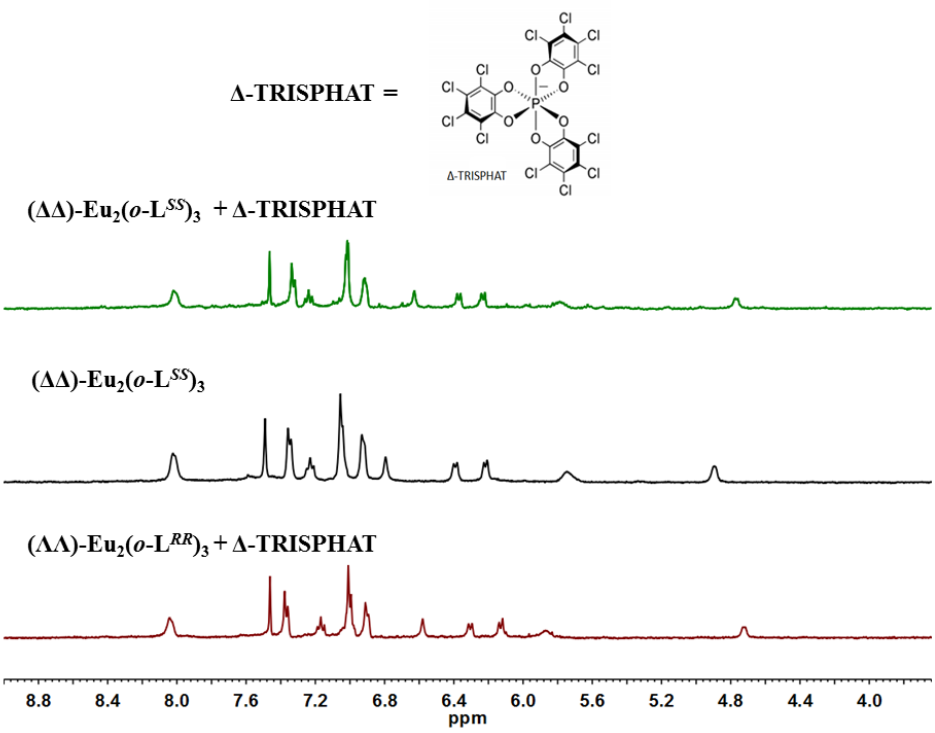

Figure S 14 ^{1}H NMR enantiomeric differentiation experiments for the enantiomers of (ΛΛ)-Eu_2(***o*-L^{RR}**)$_3$, and (ΔΔ)-Eu_2(***o*-L^{SS}**)$_3$ by addition of 3 equiv. chiral resolving agent Δ-TRISPHAT.

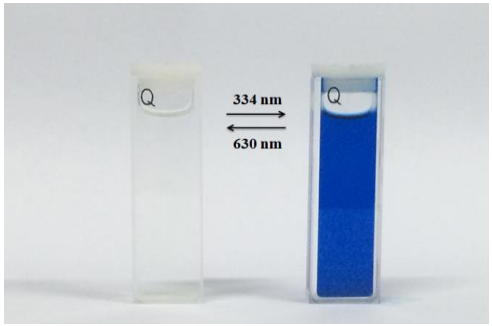

Figure S 15 The photochromic process of the ligand **L^{RR}**.

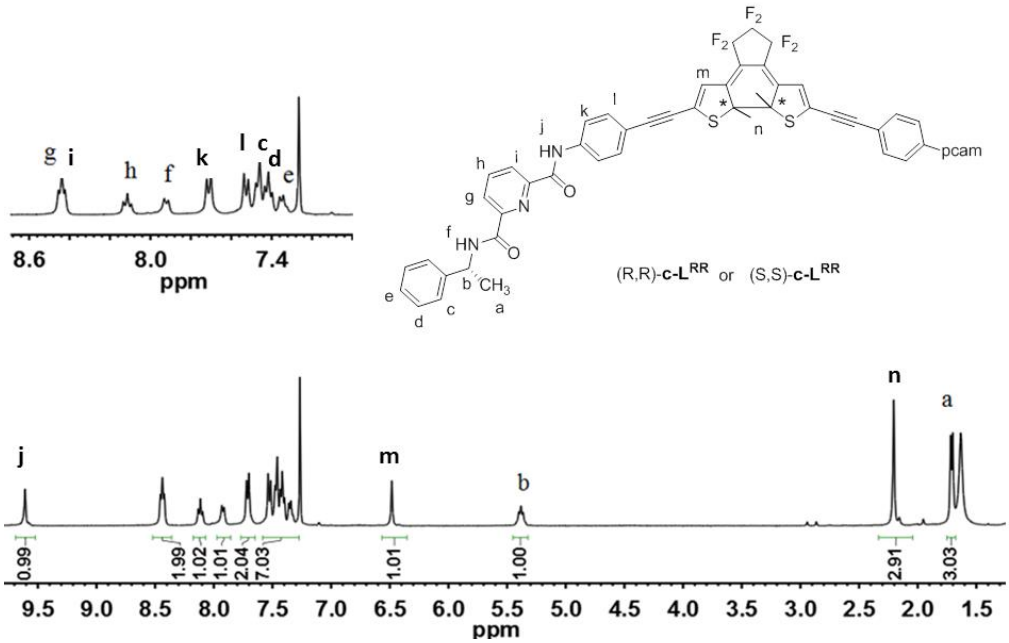

Figure S 16 ^{1}H NMR spectrum of *c*-**L**^{RR} ($CDCl_3$, 400 MHz, 293 K).

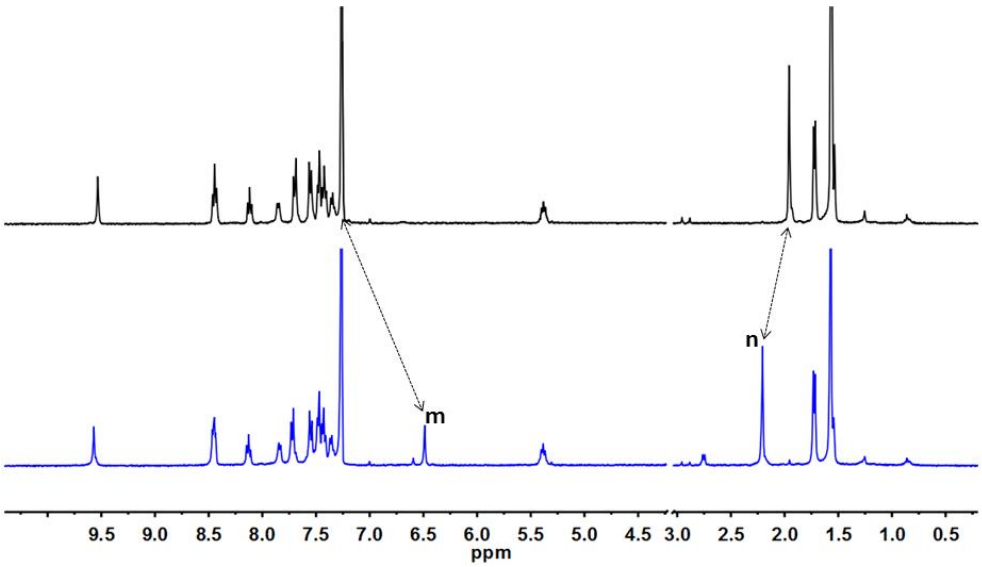

Figure S 17 ^{1}H NMR spectrum of photochromic process of ligands ($CDCl_3$, 400 MHz, 293 K).

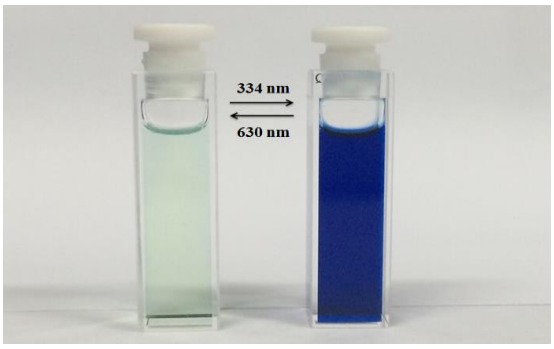

Figure S 18 The photochromic process of the helicate $[Eu_2(\boldsymbol{o}\text{-}\mathbf{L}^{\boldsymbol{RR}})_3](ClO_4)_6$.

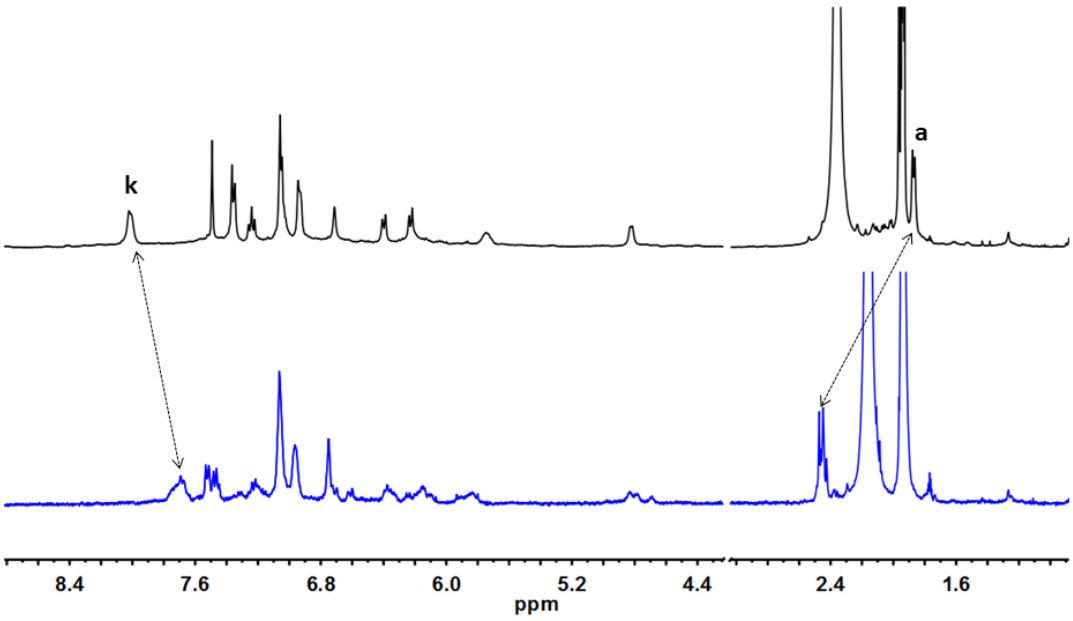

Figure S 19 ^{1}H NMR spectra of photochromic process of the helicate $[Eu_2(\boldsymbol{o}\text{-}\mathbf{L}^{\boldsymbol{RR}})_3](ClO_4)_6$ (CD_3CN, 400 MHz, 293 K).

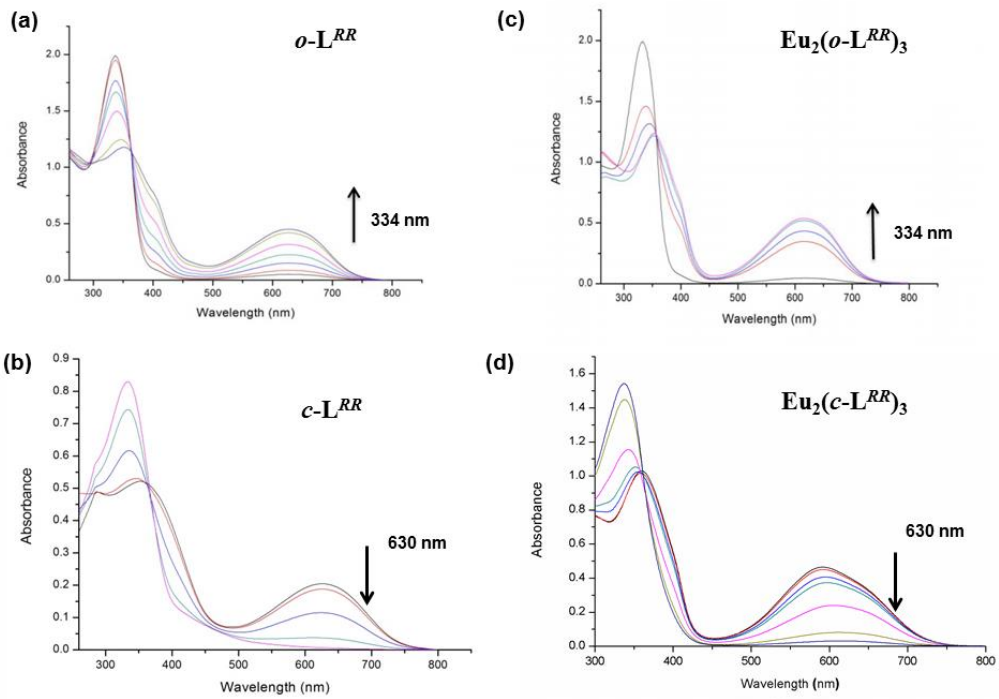

Figure S 20 UV-Vis spectra changes of ***o*-L^{RR}** in $CHCl_3$ solution upon irradiation of 334 nm light (a) and corresponding ***c*-L^{RR}** upon irradiation of 630 nm light (b); UV-Vis spectra changes of Eu_2(***o*-L^{RR}**)$_3$(ClO_4)$_6$ in CH_3CN solution upon irradiation of 334 nm light (c) and corresponding Eu_2(***c*-L^{RR}**)$_3$(ClO_4)$_6$ upon irradiation of 630 nm light (d).

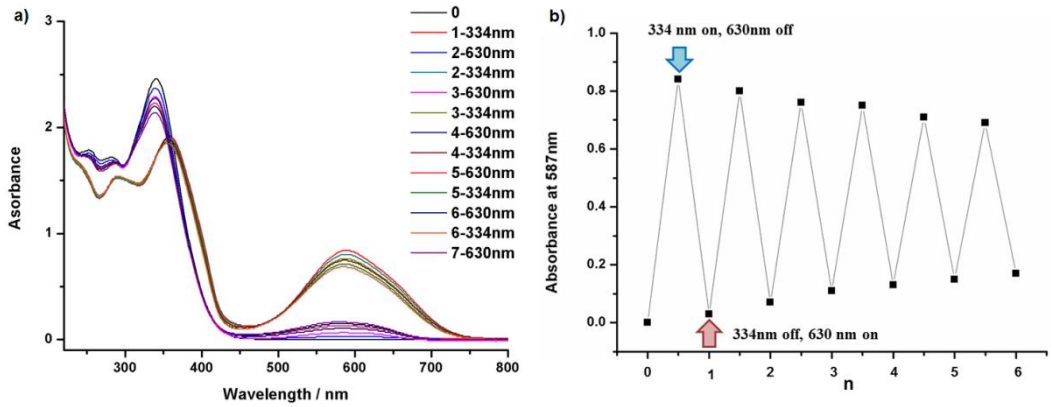

Figure S 21 UV-Vis absorbance changes of Eu_2(***o*-L^{SS}**)$_3$(ClO_4)$_6$ in CH_3CN solution on alternate excitation at 334 and 630 nm over six cycles at 293 K.

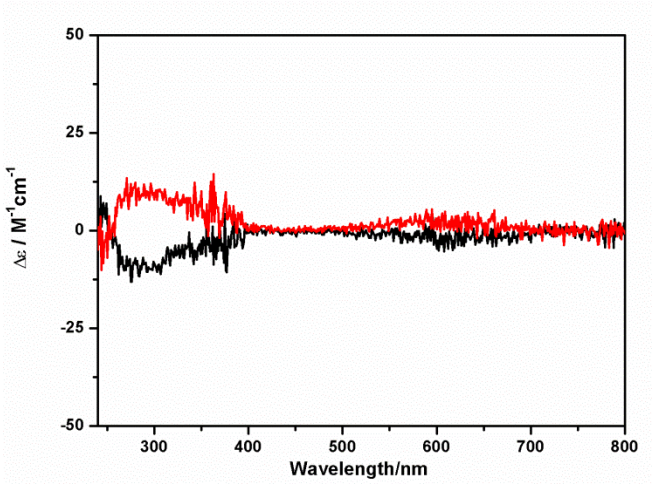

Figure S 22 CD spectra of the extracted ring-closed ligands ***c*-L^{RR}** (black line) and ***c*-L^{SS}** (red line) from the helicates (5×10^{-5} M, $CHCl_3$, 293K).

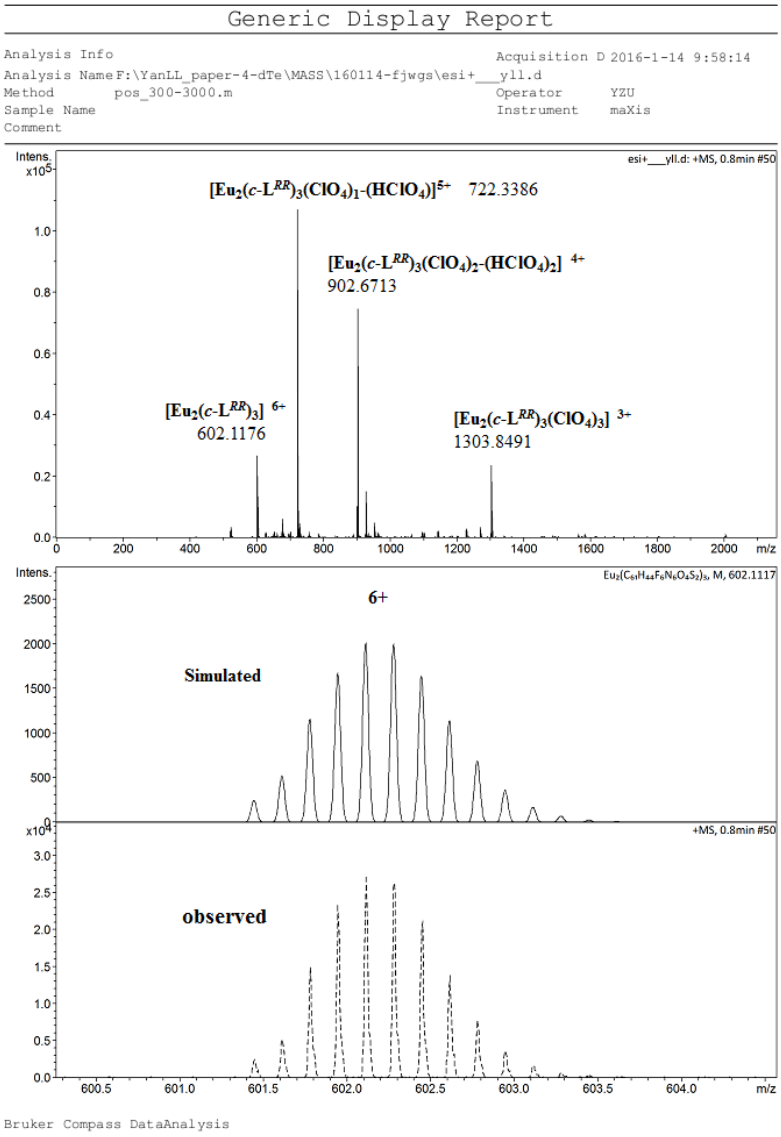

Figure S 23 ESI-TOF-MS spectrum for the ring-closure helicate Eu_2(***c*-L^{RR}**)$_3$(ClO_4)$_6$.

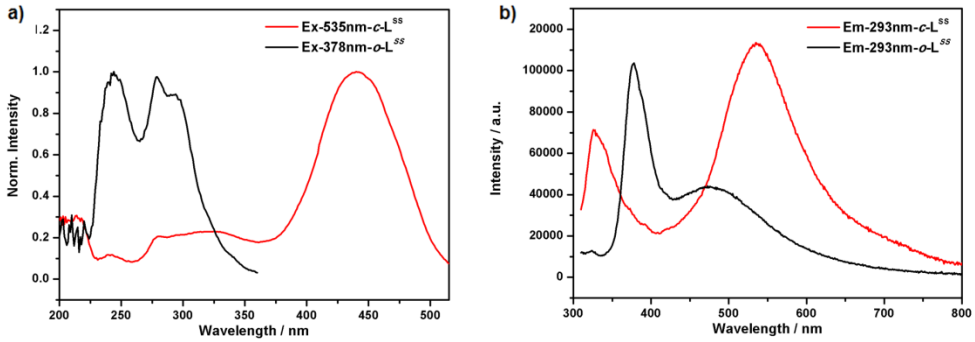

Figure S 24 Excitation and emission spectra of ***o*-L^{SS}** (black) and corresponding ring-closure product ***c*-L^{SS}** upon irradiation of 334 nm in $CHCl_3$ (3×10^{-4} M).

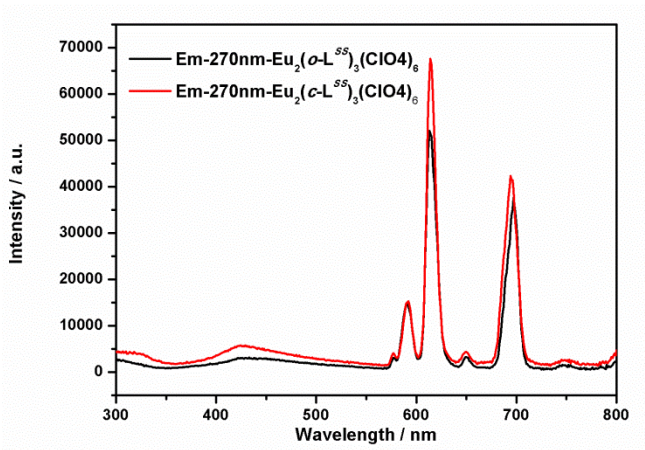

Figure S 25 Emission spectra of Eu_2(***o*-L^{SS}**)$_3$(ClO_4)$_6$ and corresponding ring-closure product Eu_2(***c*-L^{SS}**)$_3$(ClO_4)$_6$ in CH_3CN solution (1×10^{-4} M) (λ_{ex} = 270 nm).

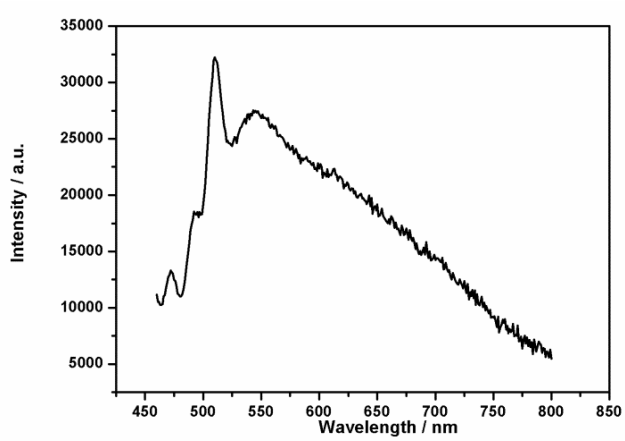

Figure S 26 Emission spectra of ring-closure product Eu_2(***c*-L^{SS}**)$_3$(ClO_4)$_6$ when exited at 441nm.

3. References

S1. a) S. Fraysse, C. Coudret, J. P. Launay, Eur. J. Inorg. Chem. 2000, 1581; b) B. He, O. S. Wenger, J. Am. Chem. Soc. 2011, 133, 17027.